Nanoscale

PAPER

View Article Online
View Journal | View Issue

Check for updates

Cite this: *Nanoscale*, 2023, **15**, 5696

Improving anion-exchange efficiency and spectrum stability of perovskite quantum dots *via* an Al^{3+} bonding-doping synergistic effect†

Linxiang Yang,‡ Qingsong Shan,*‡ Shuai Zhang, Yihui Zhou, Yan Li, Yousheng Zou and Haibo Zeng *

Received 17th December 2022,
Accepted 1st February 2023

DOI: 10.1039/d2nr07091j

rsc.li/nanoscale

Anion-exchange reactions are recognized as a vital and facile post-synthesis method to precisely manipulate the emission spectra of perovskite quantum dots (QDs). However, the anion-exchange process often induces adverse structural evolution and trap-mediated mechanisms, so mixed-halide perovskite QDs suffer inefficient anion exchange and poor spectra-stability issues, which limits access to high-quality primary color perovskite QDs for display applications. Here we report an Al^{3+} bonding-doping synergistic strategy for manufacturing stable mixed Br/Cl deep-blue perovskite QDs. By doping Al^{3+} into perovskite QDs, highly-efficient Cl^- anion exchange and a large-range blue shift of the PL spectrum (~62 nm with only 0.1 mmol of Cl feed) can be easily achieved. Notably, the Al^{3+}-mediated deep-blue emission sample exhibits superior stability against moisture and electric fields. It also shows an elevated valence band maximum level. Based on the anion-exchanged QDs, a spectrum-stable deep-blue QLED with an EQE of 1.38% at 463 nm is achieved. Our findings demonstrate a feasible and promising strategy for developing high-performance deep-blue perovskite materials and optoelectronic devices.

Published on 12 1401. Downloaded on 31/03/1403 11:14:43 ..

1. Introduction

Perovskite quantum dots (QDs), which exhibit unique advantages, especially excellent color purity and high photoluminescence quantum yields, stand out as promising photoelectronic semiconductors in light-emitting diodes (LEDs),[1–4] solar cells (SCs),[5–7] photoelectric detectors (PDs),[8] *etc*. Significant progress has been achieved for LEDs based on perovskite QDs.[9,10] Green and red perovskite QD light-emitting diodes (QLEDs) have shown external quantum efficiencies (EQEs) of over 20%,[11–13] and the EQE of blue perovskite QLEDs has reached 10%.[14–16] However, the development of deep-blue perovskite LEDs still lags significantly behind because of the difficulty of synthesizing high-quality deep-blue emission mixed-halide perovskite QDs, and the mismatched energy levels in the QLEDs.

It is well known that the spectra of perovskite QDs can be easily adjusted by changing the halogen composition to cover nearly the whole visible range. Most of the perovskite QDs with RGB primary colors used for display applications are achieved by mixing halogens to change the I/Br or Cl/Br proportion in the QDs, either in a lead-halide precursor or post-processing anion exchange.[4] Anion exchange has shown excellent applicability for fabricating primary color perovskite QLEDs.

An accepted mechanism of anion exchange involves the diffusion-limited theory,[17,18] in which the exchange is spontaneous and fast due to a large activation energy and high surface reaction constant.[19] Generally, the extent of anion exchange is related to the chemical potential (such as the concentration gradient or binding-energy difference).[20,21] Because of the lattice constant change and ligand dissociation, anion exchange exhibits limited benefits for improving the performance of QDs. There are several shortcomings for typical anion exchange: first, limited exchange – an extensive range of adjustment requires the assistance of a polar solvent of more halogen sources.[22] Second, the unstable chemical state of the surface – defects arise from the substitution of anions and ligands. A typical solution is the ligand-assisted strategy, which provides a halogen source and can effectively decrease the superficial defects of QDs during the post-synthesis process.[23,24]

The shortcomings discussed above are unfavorable for the preparation of high-quality QDs. Therefore, most research still focuses on reducing the anion exchange-induced instability of perovskite QDs, especially the spectral shift and performance degradation of QDs and LEDs.[25] However, the influence of the exchange efficiency on stability is rarely mentioned. Research

MIIT Key Laboratory of Advanced Display Materials and Devices, Institute of Optoelectronics & Nanomaterials, School of Materials Science and Engineering, Nanjing University of Science and Technology, Nanjing 210094, China. E-mail: shanqingsong@njust.edu.cn, zeng.haibo@njust.edu.cn

†Electronic supplementary information (ESI) available. See DOI: https://doi.org/10.1039/d2nr07091j

‡These authors contributed equally.

This journal is © The Royal Society of Chemistry 2023

Published on 12 1401. Downloaded on 31/03/1403 11:14:43 ..

into the promotion of the efficiency of anion exchange by chemical synthesis, especially by cation doping, lags behind. In previous works, the interaction between the doping cations and halogens, especially its impact on halide exchange in the post-processing stage, is usually ignored.[26–28]

Here we report a new method for manufacturing mixed Br/Cl blue perovskite QDs based on the Al^{3+} bonding-doping synergistic effect and anion-exchange strategy. By introducing aluminum salt in the synthesis stage, a large-range blue shift of the PL spectrum (~62 nm with a 1 : 1 ratio of Al/Pb) can be easily achieved after the anion-exchange process (with 0.1 mmol of Cl ligands). Notably, the Al-doped sample exhibited superior stability against moisture and electric field. Based on the Al-doped perovskite, we fabricated a stable deep-blue LED (463 nm) with an EQE of 1.38%. This method provides a feasible and promising strategy for preparing high-efficiency and stable blue perovskite QDs and their optoelectronic devices.

2. Experimental

2.1. Materials and reagents

Caesium carbonate (Cs_2CO_3, Macklin, 99.999%), lead bromide ($PbBr_2$, Aladdin-reagent, 99.99%), $PbCl_2$ (Aladdin-reagent, 99.99%), aluminum(III) acetylacetonate ($Al(acac)_3$, Aladdin-reagent, 99.99%), tetra-*n*-octylammonium bromide (TOAB, from Macklin), didodecyl (dimethyl) azanium bromide (DDAB, Aladdin-reagent, 98%), didodecyl (dimethyl) azanium chloride (DDAC, Aladdin-reagent, 98%), oleic acid (OA, Aladdin-reagent, 90%), *n*-octanoic acid (OTAc, Macklin, 99%), 4-dodecylbenzenesulfonic acid (DBSA, Aladdin-reagent, 90%), *n*-octane (Aladdin-reagent, 95%), toluene (Sinopharm Chemical Reagent Co., Ltd, AR), butyl acetate (Macklin, 99%), LiF, Al, poly(bis(4-phenyl)(2,4,6-trimethylphenyl) amine) (PTAA), 1,3,5-tris(1-phenyl-1*H*-benzimidazol-2-yl)benzene (TPBi) and PEDOT : PSS solutions (Baytron P VPAl 4083, filtered through a 0.45 μm filter) were purchased from Xi'an Polymer Light Technology Corp.

2.2. Synthesis of perovskite QDs

The synthesis of perovskite QDs is based on previous literature and modifications.[12,29] First, preparation of the Cs precursor: 1 mmol of Cs_2CO_3, 2.5 mL of OTAc and 5 mL of DBSA are mixed and stirred at room temperature until complete dissolution. Second, deployment of the Pb precursor solution: 1 mmol of $PbBr_2$ and 2.3 mmol of TOAB are dissolved in 40 mL of toluene. For the synthesis of $CsPbBr_3$ QDs, 0.5 mL of a cesium precursor solution is quickly added into 10 mL of the Pb–Br precursor solution in a conical flask. The solution is magnetically stirred for 2 min at room temperature in the open air. Subsequently, 3 mL of DDAB (~0.1 mmol in toluene) solution is added, and stirring continues for two more minutes. To synthesize Al-doped QDs, $Al(acac)_3$ is additionally added to the Pb-precursor.

For the synthesis of mixed halogen perovskite QDs with the same emission wavelength as Al-doped QDs, the type of precursor is adjusted, the Al/Pb ratio of Al-doped QDs is modified to 1 : 2, and the Pb-precursor of the mixed halogen perovskite QDs is modified to $PbBr_2/PbCl_2$ = 2 : 3.

2.3. Purification and anion exchange process of perovskite QDs

The purification and anion exchange processes are consistent between the control and Al-doped samples. The crude solution was mixed with butyl acetate (volume ratio of 1 : 2) and centrifugated at 8000 rpm for 1 min to acquire purified $CsPbBr_3$ QDs. Then, the precipitate was dispersed in toluene, and 3 mL of DDAC (0.1 mmol in toluene) and 0.1 mmol of OA were added for anion exchange. A double volume of butyl acetate was used to purify the QDs for the second time. The precipitate was finally dispersed in 4 mL of *n*-octane to form stable QD inks.

For the synthesis of deep-blue emission QDs, a wavelength of 463 nm was selected. The amount of DDAC for anion exchange was fixed at 0.15 mmol for both Al-doped and mixed halogen QDs.

2.4. Device fabrication

The device structure is PEDOT : PSS/PTAA/QDs/TPBi/LiF/Al. The parameters are as follows: PEDOT : PSS solutions (Baytron P VPAl 4083, filtered through a 0.45 μm filter) are spin-coated onto ITO substrates (3000 rpm for 45 s) and baked (140 °C for 15 min). PTAA solutions (in chlorobenzene, 5 mg mL^{-1}) are subsequently spin-coated (3000 rpm for 45 s) and baked (120 °C for 20 min), and the QDs are spin-coated at 2000 rpm for 45 s. LiF/Al electrodes (1 nm/100 nm) are deposited under a high vacuum of 2×10^{-4} Pa by a thermal evaporation system. The active area was 9 mm^2, as defined by the overlapping area of the ITO and Al electrodes.

2.5. Characterization and device measurements

HR-TEM photographs were acquired by a JEOL JEM 2100F-AC transmission electron microscope (TEM) with an acceleration voltage of 200 kV. XRD patterns were acquired using a Bruker D8 Advance X-ray diffractometer operating with Cu Kα radiation (λ = 1.5406 Å). The absorbance and PL spectra of the QD solution were obtained by a Shimadzu UV-3600 spectrophotometer and Varian Cary Eclipse spectrometer. XPS spectra were recorded on a Thermo ESCALAB-250 spectrometer (monochromatic Al-KR radiation source), and the XPS samples were prepared onto Si wafers. The PL decay was measured with an excitation wavelength of 365 nm (Hamamatsu C11367 Quantaurus-Tau system). The electroluminescent (EL) characteristics were analyzed by an LED test system (Everfine Photo-E-Info Co., Ltd) containing a Keithley 2400 light source instrument and Konica Minolta CS-2000 spectrometer.

3. Results and discussion

3.1. Efficient exchange in ACPB QDs

The synthesis of the QDs is modified from previous references with a room-temperature synthesis method,[12,29] followed by anion exchange to achieve the adjustment of the blue-emission

Published on 12 1401. Downloaded on 31/03/1403 11:14:43 ..

spectra. The perovskite structures of $CsPbBr_3$ and $CsPbBr_3$:Al form in the synthesis stage, and the Cl^- enters the lattice by the subsequent post-synthesis anion-exchange treatment for preparing blue perovskite QDs ($CsPb(Br/Cl)_3$ and $CsPb(Br/Cl)_3$:Al). Here, we named the $CsPbBr_3$, $CsPbBr_3$:Al, $CsPb(Br/Cl)_3$ and $CsPb(Br/Cl)_3$:Al QDs as CPB, ACPB, CPBC, and ACPBC, respectively. Schematic diagrams of the two anion-exchange processes are shown in Fig. 1, before which the Al salt was added to the Pb-precursor. According to a previous report, when Al^{3+} is doped in $CsPbBr_3$ QDs, two Al^{3+} occupy the site of one Pb^{2+} and form a tetra-coordinated $[Al_2Br_6]$ octahedral structure,[30] where the ionic radii of Pb^{2+} and Al^{3+} are 119 pm and 53.5 pm. In particular, the crystal structure of room temperature synthesized $CsPbX_3$ QDs is orthorhombic, and has more space along one of the axes,[31] hence Al-doping leads to a contracted lattice.[27]

During the anion exchange process, there are several factors worth noting. First, as a surface chemically dependent material, the environment of the terminating atoms on the QD surface is important. Surface defects may facilitate the anion exchange process.[32,33] With the assistance of the DDAC ligand, Cl exchanges with halogens in the $[Pb\text{-}Br_6]^{4-}$ octahedron to form $[Pb\text{-}(Br/Cl)_6]^{4-}$ (Fig. 1a).[16] The process is spontaneous, and the main driving force is the chemical potential gradient (concentration gradient). Furthermore, the unique structure of the [Al–Cl] octahedra and the strong synergistic effect between $Al^{3+}$and Cl^- (Fig. 1b) result in efficient anion exchange. Al^{3+} in the crystal is more inclined to bond to Cl^-, which provides an additional exchange driving force, and reduces the diffusion barrier of Cl^-, attracting more Cl ions to enter the lattice. A more efficient anion exchange is realized in a shorter time and with superior stability. Hence, the Al^{3+} bonding-doping synergistic effect is suitable for subsequent high-efficiency anion exchange in blue, especially deep-blue, perovskite.

As a result of the synergistic effect, the photoluminescence (PL) spectra of the ACPB QDs after anion exchange show a large-range blue shift (Fig. 2a). This high-efficiency process is highly dependent on the feed ratio of the Al^{3+} species. With an Al : Pb feed ratio of 1 : 1, the ACPBC QDs exhibit emission at 440 nm after Cl-anion exchange with only 0.1 mmol of DDAC, while the anion-exchanged CPBC QDs exhibit PL emission at 502 nm (Fig. 2a). It is clear that the anion-exchange spectral adjustments of the ACPBC QDs are continuous, and the blue shifts are more pronounced compared with those for CPBC. As the ratio of Al^{3+} increases, the spectra of the anion-exchanged ACPBC QDs gradually shift to shorter wavelengths, as shown in Fig. 2b, and the emission of ACPBC blue shifts to the deep-blue range.

According to previous works, Al^{3+} itself may cause the spectrum of $CsPbBr_3$ to shift to a shorter wavelength when using the hot-injection method.[30] To rule out blue shift resulting from the effect of Al doping in the $CsPbBr_3$ lattice, the initial solutions of QDs before anion exchange are tested (Fig. S1a†). Interestingly, the spectra of the QDs during the synthesis process demonstrate only a slight blue shift of 10 nm with Al/Pb = 1 : 1 (green line in Fig. 2c). The blue shifts of the other samples with less Al^{3+} are negligible. Such a small blue shift can be attributed to the difference in the synthesis method (a

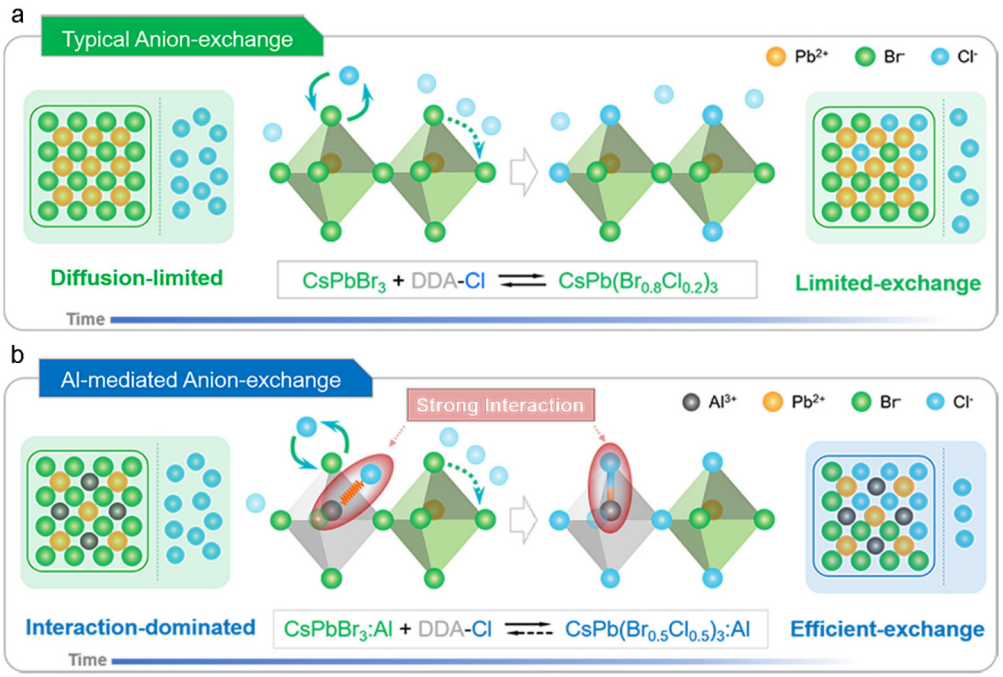

Fig. 1 (a) Schematic diagram of the anion exchange process for typical CPB QDs. (b) Schematic diagram of the anion exchange process for ACPB QDs. The additional exchange driving force is a synergistic strong covalent interaction resulting from Al doping, which leads to a more efficient and thorough anion exchange process.

 This journal is © The Royal Society of Chemistry 2023

Published on 12 1401. Downloaded on 31/03/1403 11:14:43 ..

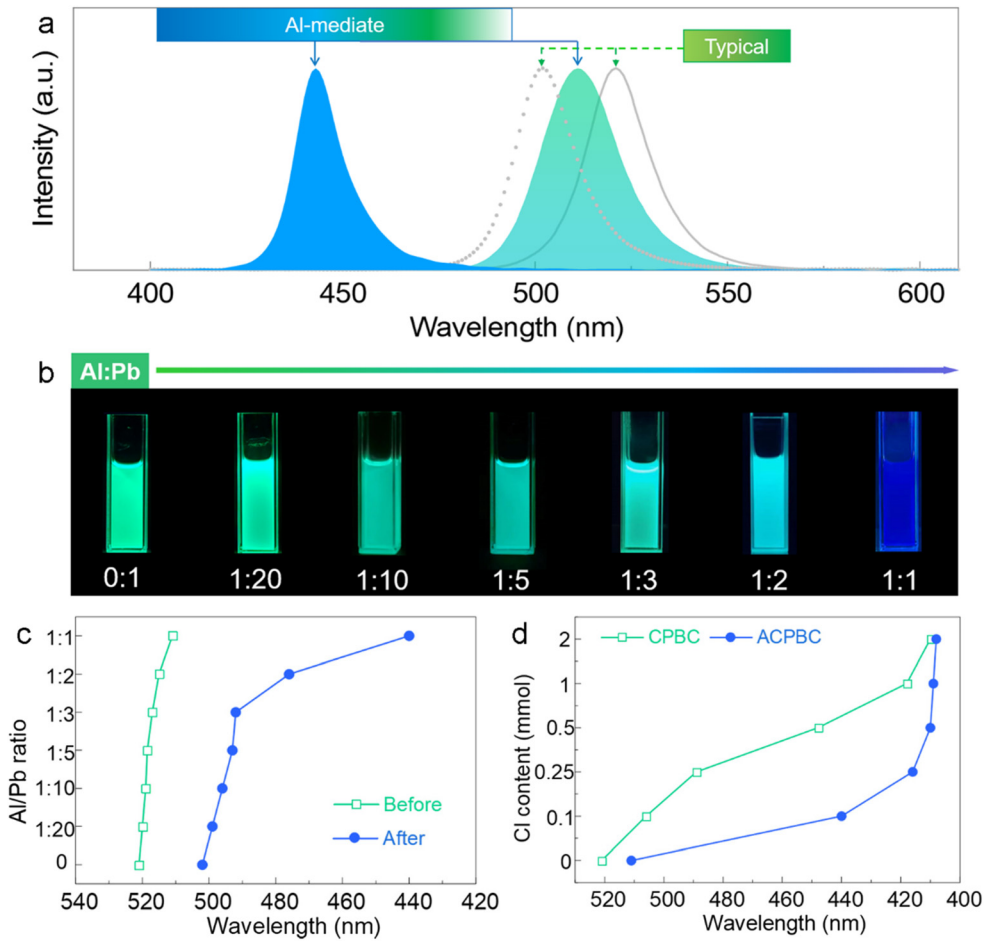

Fig. 2 (a) The PL spectra of typical (CPB and CPBC) and Al-mediated (ACPB and ACPBC) samples. (b) Pictures of the QDs under ultraviolet light. The amounts of Pb in the precursor and Cl in the anion exchange are fixed (0.1 mmol). Upon increasing the amount of Al in the Pb-precursor, the PL blue shifts to the deep-blue range. (c) The emission peaks of various ACPB QDs before (green) and after (blue) anion exchange. (d) The emission peaks after anion exchange of CPB (green) and ACPB (blue) QDs with different amounts of DDAC. The Al/Pb ratio is fixed at 1 : 1.

room-temperature synthesis method is used in this article) and a slight lattice contraction caused by Al^{3+} doping. This phenomenon proved that the noticeable change in PL is because of the Cl-anion exchange assisted by a strong bonding-doping synergistic effect of Al and the halogen (Fig. S1b†).

Fig. 2c and d demonstrate the different anion exchange limitations for CPB and ACPB. First, ACPBC QDs consistently exhibit a stronger blue-shift effect, and the difference is still apparent when more Cl sources are added to the anion exchange system. There remains a difference of 63 nm with 0.2 mmol of DDAC addition. Simultaneously, the ACPBC reaches the anion exchange limit earlier, which is because of the inherent properties of the QDs. If excess Cl is mixed in the system, the effect of Al in increasing the anion exchange limit will not be obvious because the considerable chemical potential gradient hides the synergistic effect of Al^{3+} and the halogen (the blue point with Cl content of 2 mmol in Fig. 2d).

Furthermore, an equal amount of Al^{3+} (Al/Pb = 1 : 1) is added synergistically during the anion exchange process to determine whether the addition of Al in the post-treatment process can also lead to more efficient anion exchange. The solution is vigorously stirred at room temperature for 1 h to ensure an adequate reaction. As shown in Fig. S2 of the ESI,† there is no blue shift in the sample (blue line), indicating that the bonding-doping synergistic effect of Al and the halogen only occurs if Al is present in the lattice. The slight red shift of the PL may be caused by grain growth during agitation.

3.2. The structure of ACPBC QDs

To further explore the structure of ACPBC QDs, HR-TEM, XRD, and XPS are used. The microstructures of CPBC and ACPBC QDs are characterized. The HR-TEM images of two samples are shown in Fig. 3a and b, and it can be seen that the average diameters of CPBC (Fig. 3a) and ACPBC (Fig. 3b) are approximate, and the interplanar crystal spacings are 2.87 and 2.81 Å, which suggests that the blue shift of the ACPBC QDs originates from the lattice contraction caused by the Al and Cl ions in the QDs. To further investigate the existence of Al in the crystal structure of the ACPBC sample, the X-ray diffraction (XRD) pat-

Published on 12 1401. Downloaded on 31/03/1403 11:14:43 ..

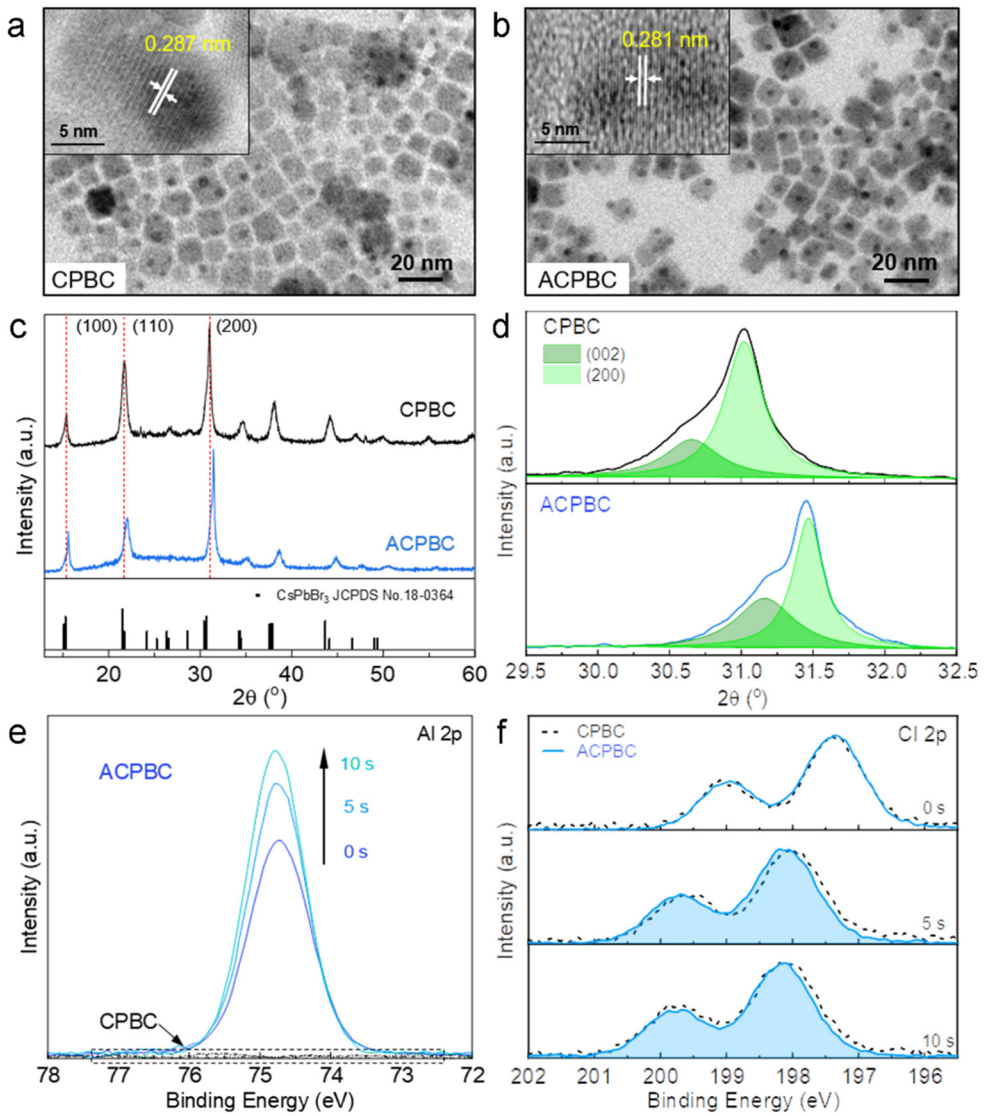

Fig. 3 (a) and (b) HR-TEM spectra of CPBC and ACPBC QDs. The insets show the interplanar crystal spacing data. (c) XRD patterns of CPBC and ACPBC QDs. The black vertical lines represent the standard card of $CsPbBr_3$ (JCPDS no. 18-0364). (d) Locally amplified data for the CPBC and ACPBC QDs with different characteristic peaks assigned. (e) XPS data for Al 2p of CPBC and ACPBC QDs. The dark blue, medium blue, and light blue curves show data after etching for 0 s, 5 s and 10 s, respectively. (f) XPS data for Cl 2p of CPBC and ACPBC QDs after etching for 0 s, 5 s and 10 s. The light blue areas represent the Cl 2p XPS peaks of ACPBC.

terns of the different samples were recorded. Fig. 3c shows the XRD spectra of the CPBC (black) and ACPBC (blue) samples and the black perpendicular lines are the characteristic peaks of standard PDF cards $CsPbBr_3$ (JCPDS no. 18-0364). It can be clearly seen that all the XRD spectra match the standard card well, indicating that the main crystal structure remains stable. As expected, the pattern of ACPBC shows a shift towards higher angles, mainly due to the high-efficiency anion exchange induced by the Al^{3+} bonding-doping synergistic effect, which allows more Cl to enter the lattice and contracted lattice. This result is consistent with the conclusions from the HR-TEM graphs that the crystal plane spacing decreases in ACPBC QDs. Meanwhile, as reported in previous work by Meng's group, the change of relative intensity ((002) and (200) for $CsPbBr_3$) originates from the lattice deformation and preferential orientation,[30] which may be one of the proofs of the stability, as discussed later.

Although we have proved the existence and structure of ACPBC QDs, whether Al^{3+} exists specifically on the surface or the interior remains inconclusive. In order to confirm the position of the Al in the QDs, we further explore the elemental XPS spectra (Fig. S3† and Fig. 3e–f). The XPS spectra of CPBC and ACPBC QDs are presented, and the changes in the binding energies in samples with Ar^+ ion-etching are observed. As shown in Fig. 3e, the XPS peak of Al is only found in the ACPBC QDs, which means that the efficient anion exchange achieved is assisted by Al. After being etched for 5 s, the intensity of Al is greater than that of the untreated sample, and the

 This journal is © The Royal Society of Chemistry 2023

Published on 12 1401. Downloaded on 31/03/1403 11:14:43 ..

binding-energy peak shifts to higher energy. With continued etching, the peak position moves slightly. This result indicates that the gradient distribution of Al in the QDs is consistent with better bonding and fewer defects inside the QDs.

The XPS data for Cl indicates the bonding situation of Cl and the cations (Pb and Al). The spectra are shown in Fig. 3f. Except for at the interface, the ACPBC QDs exhibit stronger bonding than the CPBC QDs, because there are fewer defects in the internal layer and a stronger bond between Cl^- and the metal cation (mainly Al^{3+} and Pb^{2+}).[34] There are almost no differences between the CPBC and ACPBC surfaces, probably because of the surface DDA^+ ligands bonding to Cl^- and passivating the surface defects.[34] Correspondingly, the peaks of the Br spectra (Fig. S3b†) for the ACPBC QDs show weaker binding energies than those for the CPBC QDs, which is consistent with the previous argument that Br is more likely to bond to Pb in our system.

Interestingly, the XPS spectra of Pb in the CPBC and ACPBC QDs are different (Fig. S3c†). There are peaks attributed to Pb^0 (~136.7 eV) in the curves of the CPBC QDs etched for 5 s and 10 s, but there are no such peaks for the ACPBC QDs, which is because of phase decomposition by high-energy electrons.[35] This phenomenon can be explained by weaker lattice stability of the CPBC QDs, and the characterizations will be discussed in detail later.

3.3. The stability of anion-exchanged ACPBC QDs

Generally, higher-stability QDs demonstrate well-distributed growth dynamics. The *in situ* PL spectra can explain the uniformity of the QDs to a certain extent. Interestingly, Al-doping results in more stable and even crystal growth. The *in situ* PL spectra of the CPB and ACPB QDs are shown in Fig. S4a and b.† During the synthesis process, the CPB QDs exhibit two emission peaks at 518 and 534 nm, while the ACPB QDs exhibit a single peak at 510 nm. As the reaction time increases, the particle size of the QDs increases, and the entire emission spectrum is redshifted. The unevenly grown CPB QDs gradually appear with a dominant emission peak at 530 nm. At the same time, the ACPBC QDs show a slight redshift and a weakly extra peak at 530 nm, and a coarse solution of QDs with a more uniform size is finally obtained. The micrographs and size distributions of the CPB and ACPB QDs are exhibited in Fig. S4c–f,† and it can be clearly seen from the particle size statistics (Fig. S4e and f†) that the ACPB exhibits a more uniform distribution.

A precursor-mixed halogen QD with the same emission wavelength was synthesized to investigate the effect of Al^{3+} on the stabilization of the blue-emission perovskite phase. The synthesis method is described in detail in the Experimental section. For convenient description, the mixed halogen perovskite is named MCPBC. The PL wavelengths of the CPBC, ACPBC, and MCPBC QDs are 490, 460, and 460 nm.

As mentioned in the previous section, the decomposition of Pb leads to the failure of the QDs. The structure of the perovskite consists of $[PbX_6]^{4-}$ and Cs^+, and the surface ligands are chelated to halogens or surface defects. Usually, the surface of the QDs ends in [Pb-X] octahedra, and is easily damaged because of the highly dynamic anion on the surface, exposing Pb^{2+} and further leading to the decomposition and failure of the QDs.[36,37] When Al cations are doped in the crystal, the shorter bond length and stronger bonding strength can improve the lattice stability of the QDs.[27] Therefore, the Pb-XPS spectrum of the MCPBC QDs is analyzed (Fig. S5†), and it can be clearly seen that the peak intensity attributed to Pb^0 is significantly higher than those of the ACPBC and CPBC QDs, indicating lower stability than the CPBC and ACPBC QDs.

The moisture stability of the QDs is tested by storing the QDs in water. Due to the corrosive effect of highly polar water on perovskites, QDs tend to exhibit unstable phase decomposition and spectral changes. As shown in Fig. 4a, the PL wavelength of the CPBC QDs red-shifted to 495 nm, and that of the MCPBC QDs blue-shifted to 455 nm, which indicates that phase separation occurred. With increased storage time in the water, Al-free (CPBC and MCPBC) QDs showed worse phase decomposition and eventual failure, while ACPBC QDs exhibited suppressed spectral drift and phase decomposition. As shown in Fig. 4b, the MCPBC and CPBC QDs failed on the 7th and 10th day, respectively, while the ACPBC QDs showed better moisture stability. Information on the relative PL intensities of the QDs is provided in Fig. S6.† The intensity decreases in MCPBC and CPBC are more severe, and they fail within shorter storage times. The results of the stability against moisture illustrate that the Al^{3+} bonding-doping synergistic effect improves the stability of the QDs, and it can be predicted that the moisture stability of the QDs will be improved upon combination with other means of defect passivation.[38,39]

The temperature-dependent PL curves are observed to illustrate the lattice stability of the QDs. Consistent with reports in the literature, the $CsPb(Br/Cl)_3$ QDs exhibit a single emission peak.[40] The lattice thermal expansion due to temperature increase reduces the overlap between the Pb-6s and Br-3p/Cl-2p antibonding atomic orbitals, leading to an increase in the band gap of the QDs.[40,41] Hence, the degree of spectral blue shift can directly reflect the extent of lattice expansion. The blue shift of the ACPBC QDs is 3 nm, smaller than that of MCPBC (10 nm) and CPBC (8 nm), indicating that the strong covalent interaction of Al–Cl can stabilize the structure of the QDs.

Perovskite QDs with better stability usually have lower defect density and thus exhibit a relatively long radiative-recombination lifetime. The time-resolved photoluminescence (TRPL) of the QDs is analyzed to characterize the defects of the QDs. It can be concluded that Al^{3+} doping effectively reduces the defects of the ACPBC QDs. As shown in Fig. 4f, the dual exponential fit method is adopted to calculate the lifetime of the QDs, and the detailed results are shown in Table S1.† The Al^{3+}-doping increased the ratio of radiative recombination, which manifested as an increase of A_2 and τ_2. Meanwhile, MCPBC exhibits a higher A_2 than CPBC. As the Cl content increases, the original shallow level defects may become deep level defects, indicating the weaker ability to capture carriers

Published on 12 1401. Downloaded on 31/03/1403 11:14:43 ..

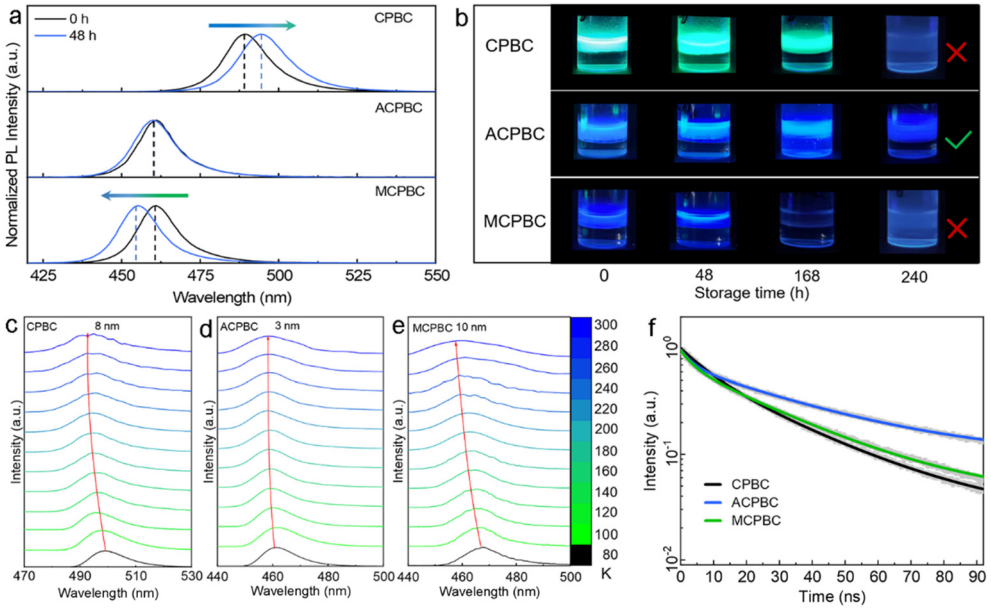

Fig. 4 (a) PL comparison of the CPBC, ACPBC, and MCPBC QDs after storing in water for 48 h. (b) Pictures of CPBC, ACPBC, and MCPBC under ultraviolet light after storing in water for 0, 48, 168 and 240 h. (c–e) Variations in the PL spectra for the CPBC, ACPBC, and MCPBC QDs. The red lines represent the changes of the peak positions with temperature elevation. (f) TRPL curves and fitting results of the CPBC (black), ACPBC (blue), and MCPBC (green) QDs.

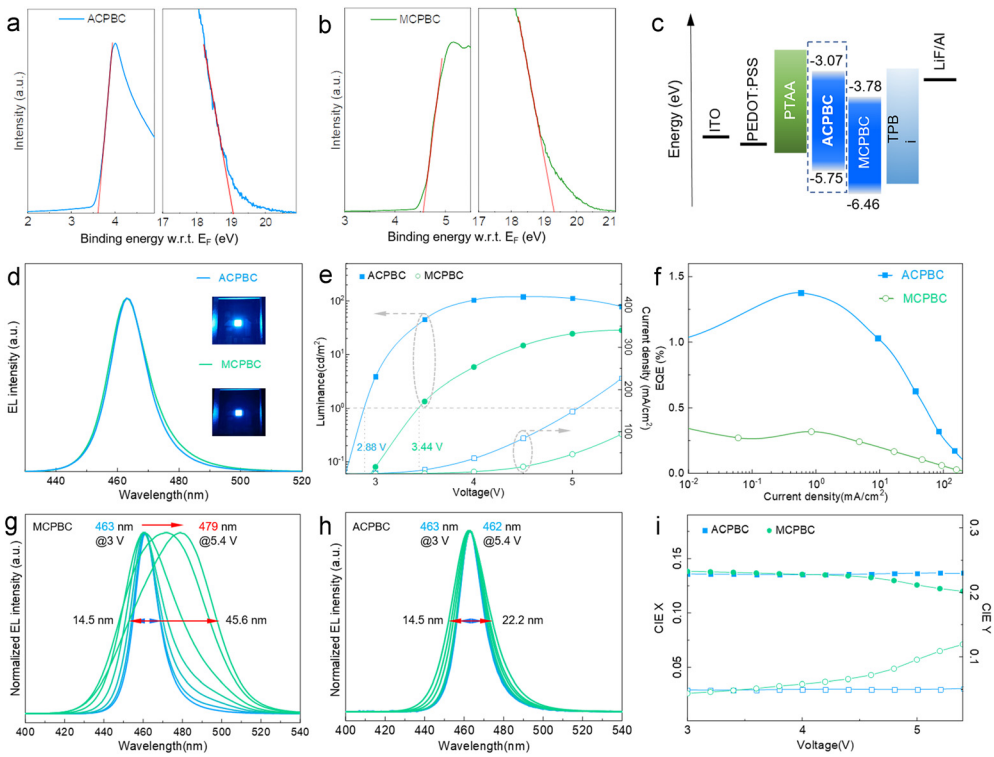

Fig. 5 (a) and (b) UPS data for the ACPBC and MCPBC QDs. The left and right tangent positions represent the secondary electron cutoff energy and electron injection barrier, respectively. (c) The device structure of the QLED and the energy level positions of the ACPBC and MCPBC QDs. (d) EL spectra (light on) of the ACPBC and MCPBC QDs. The insets show pictures of the devices at 5 V. (e) and (f) Luminance-voltage-current density and EQE-current density of the ACPBC and MCPC QDs. (g) and (h) Normalized EL spectra transformations with increasing voltage. (i) Changes of CIE X and CIE Y with voltage. The blue and green dots represent ACPBC and MCPBC, respectively.

This journal is © The Royal Society of Chemistry 2023

Published on 12 1401. Downloaded on 31/03/1403 11:14:43 ..

near the conduction and valence bands.[42] The τ_2 of ACPBC is much longer than that of CPBC and MCPBC, which is because there are fewer defects and better radiative recombination. The average lifetime (τ_{avg}) of ACPBC is 57.21 ns, higher than that of MCPBC (36.14 ns) with the same emission (460 nm in PL), which indicates that the strong Al–Cl interaction formed by the synergistic effect improves the radiative-recombination ability, revealing the potential for preparing high-efficiency deep-blue QLEDs.

3.4. Deep-blue QLEDs based on ACPBC QDs

Based on the superior stability and lower density of defect states, the ACPBC QDs are suitable for fabricating deep-blue QLEDs. The bandgap and energy level are first determined. The ultraviolet photoelectron spectra (UPS) of ACPBC and MCPBC are shown in Fig. 5a and b, and the secondary electron cutoff energy and onset of the UPS spectra for the two samples are 19.06 and 3.61, and 19.30 and 4.56 eV, respectively. Combined with the bandgap acquired from the absorption spectra in Fig. S7† (2.68 eV), the valence-band maximum (VBM) and conduction-band minimum (CBM) are calculated to be −5.75 and −3.07 eV (ACPBC), and −6.46 and −3.78 eV (MCPBC). The device structure is a classical scheme, as shown in Fig. 5c, and the injection barrier between the hole transport layer and ACPBC is significantly lower than that for MCPBC, which suggests better charge injection and more balanced transport. The energy level of the ACPBC QDs is significantly shallower than that of MCPBC, which is probably because the doping Al^{3+} affects the interaction between Pb^{2+} and the halogen (Br^-/Cl^-). QLEDs based on ACPBC and MCPBC are fabricated, and the EL performances are compared in detail. The EL peaks of the two QDs are the same at 463 nm, and the ACPBC QDs perform better. As shown in Fig. 5d, the FWHM of the QCPBC QLEDs is 14.2 nm, and the inset demonstrates the higher luminance of ACPBC at 5 V. Fig. 5e exhibits the luminance–voltage–current density curves of two QDs, and it is clear that the luminance of ACPBC (120 cd m^{-2}) is nearly five times that of MCPBC (24 cd m^{-2}). ACPBC shows a superior light-on voltage of 2.88 V, and the EQE-current density curves show an EQE of 1.38% (Fig. 5f), which is higher than that of MCPBC.

Furthermore, the ACPBC QDs demonstrate better spectral stability under a voltage. The EL spectra of ACPBC and MCPBC are shown in Fig. 5g and h. The MCPBC exhibits severe spectra drift (463–479 nm) and broadening (14.5–45.6 nm). In comparison, the FWHM of ACPBC merely increases from 14.5 nm to 22.2 nm, the peak position does not change (463 nm), and the X and Y chromaticity coordinates of the ACPBC QDs in Fig. 5i scarcely change with voltage, which illustrates superior stability under voltage.

4. Conclusions

In conclusion, we have demonstrated a new method for manufacturing stable blue perovskite QDs based on the Al^{3+} bonding-doping synergistic effect and efficient anion exchange. By introducing aluminum salt in the synthesis stage, a large-range blue shift of the PL spectrum (~62 nm with a 1 : 1 ratio of Al/Pb) is easily achieved after the anion-exchange process (with 0.1 mmol of Cl-ligands) with the assistance of strong Al–Cl bonding. The structure and binding energy characterization prove that the strong Al–Cl interaction effectively promotes Br–Cl anion exchange and stabilizes the lattice structure. Notably, benefiting from the superior bonding-doping synergistic strategy, the ACPBC QDs exhibit superior stability against moisture and an electric field. Based on the Al-doped perovskite, we fabricated a deep-blue LED (463 nm) with an EQE of 1.38% and good spectral stability. Our findings indicate a feasible and promising strategy for developing high-performance deep-blue perovskite materials and optoelectronic devices.

Author contributions

Linxiang Yang and Qingsong Shan contributed equally to this work. Linxiang Yang and Qingsong Shan: experiment, conceptualization, software, writing. Shuai Zhang, Yihui Zhou, Yan Li: experiment, investigation. Qingsong Shan, Shuai Zhang, Yousheng Zou and Haibo Zeng: supervision, writing – review and editing.

Conflicts of interest

There are no conflicts of interests to declare.

Acknowledgements

This work was supported by the National Natural Science Foundation of China (No. 52131304, 62204120, 61725402), NSFC-RGC (62261160392), the Fundamental Research Funds for the Central Universities (No. 30919012107), and the International Cooperation Program (BZ2020063).

References

1 X. K. Liu, W. Xu, S. Bai, Y. Jin, J. Wang, R. H. Friend and F. Gao, *Nat. Mater.*, 2021, **20**, 10–21.
2 Y.-H. Kim, S. Kim, A. Kakekhani, J. Park, J. Park, Y.-H. Lee, H. Xu, S. Nagane, R. B. Wexler, D.-H. Kim, S. H. Jo, L. Martínez-Sarti, P. Tan, A. Sadhanala, G.-S. Park, Y.-W. Kim, B. Hu, H. J. Bolink, S. Yoo, R. H. Friend, A. M. Rappe and T.-W. Lee, *Nat. Photonics*, 2021, **15**, 148–155.
3 Y. Hassan, J. H. Park, M. L. Crawford, A. Sadhanala, J. Lee, J. C. Sadighian, E. Mosconi, R. Shivanna, E. Radicchi, M. Jeong, C. Yang, H. Choi, S. H. Park, M. H. Song, F. De Angelis, C. Y. Wong, R. H. Friend, B. R. Lee and H. J. Snaith, *Nature*, 2021, **591**, 72–77.
4 J. Song, J. Li, X. Li, L. Xu, Y. Dong and H. Zeng, *Adv. Mater.*, 2015, **27**, 7162–7167.

Published on 12 1401. Downloaded on 31/03/1403 11:14:43 ..

5 W.-Q. Wu, P. N. Rudd, Q. Wang, Z. Yang and J. Huang, *Adv. Mater.*, 2020, **32**, 2000995.
6 J. Yuan, X. Ling, D. Yang, F. Li, S. Zhou, J. Shi, Y. Qian, J. Hu, Y. Sun, Y. Yang, X. Gao, S. Duhm, Q. Zhang and W. Ma, *Joule*, 2018, **2**, 2450–2463.
7 H. Wang, X. Zhang, Q. Wu, F. Cao, D. Yang, Y. Shang, Z. Ning, W. Zhang, W. Zheng, Y. Yan, S. V. Kershaw, L. Zhang, A. L. Rogach and X. Yang, *Nat. Commun.*, 2019, **10**, 665.
8 F. Pelayo García de Arquer, A. Armin, P. Meredith and E. H. Sargent, *Nat. Rev. Mater.*, 2017, **2**, 16100.
9 X. Li, Y. Wu, S. Zhang, B. Cai, Y. Gu, J. Song and H. Zeng, *Adv. Funct. Mater.*, 2016, **26**, 2435–2445.
10 M. Liu, Q. Wan, H. Wang, F. Carulli, X. Sun, W. Zheng, L. Kong, Q. Zhang, C. Zhang, Q. Zhang, S. Brovelli and L. Li, *Nat. Photonics*, 2021, **15**, 379–385.
11 Y.-K. Wang, F. Yuan, Y. Dong, J.-Y. Li, A. Johnston, B. Chen, M. I. Saidaminov, C. Zhou, X. Zheng, Y. Hou, K. Bertens, H. Ebe, D. Ma, Z. Deng, S. Yuan, R. Chen, L. K. Sagar, J. Liu, J. Fan, P. Li, X. Li, Y. Gao, M.-K. Fung, Z.-H. Lu, O. M. Bakr, L.-S. Liao and E. H. Sargent, *Angew. Chem., Int. Ed.*, 2021, **60**, 16164–16170.
12 T. Fang, T. Wang, X. Li, Y. Dong, S. Bai and J. Song, *Sci. Bull.*, 2021, **66**, 36–43.
13 C. Peng, R. Zhang, H. Chen, Y. Liu, S. Zhang, T. Fang, R. Guo, J. Zhang, Q. Shan, Y. Jin, L. Wang, L. Hou and H. Zeng, *Adv. Mater.*, 2023, **35**, e2206969.
14 Y. Dong, Y.-K. Wang, F. Yuan, A. Johnston, Y. Liu, D. Ma, M.-J. Choi, B. Chen, M. Chekini, S.-W. Baek, L. K. Sagar, J. Fan, Y. Hou, M. Wu, S. Lee, B. Sun, S. Hoogland, R. Quintero-Bermudez, H. Ebe, P. Todorovic, F. Dinic, P. Li, H. T. Kung, M. I. Saidaminov, E. Kumacheva, E. Spiecker, L.-S. Liao, O. Voznyy, Z.-H. Lu and E. H. Sargent, *Nat. Nanotechnol.*, 2020, **15**, 668–674.
15 X. Peng, B. He, H. Zheng, Z. Su, X. Li, L. Ji, T. Zhang, L. Chen, C. Qin, X. Gao, S. Li and X. Yang, *ACS Energy Lett.*, 2022, **8**, 339–346.
16 H. Zhu, G. Tong, J. Li, E. Xu, X. Tao, Y. Sheng, J. Tang and Y. Jiang, *Adv. Mater.*, 2022, **34**, 2205092.
17 B. A. Koscher, N. D. Bronstein, J. H. Olshansky, Y. Bekenstein and A. P. Alivisatos, *J. Am. Chem. Soc.*, 2016, **138**, 12065–12068.
18 Y. Zhang, D. Lu, M. Gao, M. Lai, J. Lin, T. Lei, Z. Lin, L. N. Quan and P. Yang, *Proc. Natl. Acad. Sci. U. S. A.*, 2019, **116**, 12648.
19 M. Sygletou, M.-E. Kyriazi, A. G. Kanaras and E. Stratakis, *Chem. Sci.*, 2018, **9**, 8121–8126.
20 G. H. Ahmed, J. K. El-Demellawi, J. Yin, J. Pan, D. B. Velusamy, M. N. Hedhili, E. Alarousu, O. M. Bakr, H. N. Alshareef and O. F. Mohammed, *ACS Energy Lett.*, 2018, **3**, 2301–2307.
21 M. Gong, R. Sakidja, R. Goul, D. Ewing, M. Casper, A. Stramel, A. Elliot and J. Z. Wu, *ACS Nano*, 2019, **13**, 1772–1783.
22 C. Guhrenz, A. Benad, C. Ziegler, D. Haubold, N. Gaponik and A. Eychmüller, *Chem. Mater.*, 2016, **28**, 9033–9040.
23 Y. J. Yoon, K. T. Lee, T. K. Lee, S. H. Kim, Y. S. Shin, B. Walker, S. Y. Park, J. Heo, J. Lee, S. K. Kwak, G.-H. Kim and J. Y. Kim, *Joule*, 2018, **2**, 2105–2116.
24 E. Scharf, F. Krieg, O. Elimelech, M. Oded, A. Levi, D. N. Dirin, M. V. Kovalenko and U. Banin, *Nano Lett.*, 2022, **22**, 4340–4346.
25 K. Zhang, L. X. Cao, Y. Tang, Y. Yu, Y. Shen, B. Wang, W. J. Wang, Y. Q. Li and J. X. Tang, *Laser Photonics Rev.*, 2022, 2200689.
26 S. Zou, Y. Liu, J. Li, C. Liu, R. Feng, F. Jiang, Y. Li, J. Song, H. Zeng, M. Hong and X. Chen, *J. Am. Chem. Soc.*, 2017, **139**, 11443–11450.
27 C. Bi, S. Wang, Q. Li, S. V. Kershaw, J. Tian and A. L. Rogach, *J. Phys. Chem. Lett.*, 2019, **10**, 943–952.
28 P. K. Nayak, M. Sendner, B. Wenger, Z. Wang, K. Sharma, A. J. Ramadan, R. Lovrinčić, A. Pucci, P. K. Madhu and H. J. Snaith, *J. Am. Chem. Soc.*, 2018, **140**, 574–577.
29 T. Wang, X. Li, T. Fang, S. Wang and J. Song, *Chem. Eng. J.*, 2021, **418**, 129361.
30 M. Liu, G. Zhong, Y. Yin, J. Miao, K. Li, C. Wang, X. Xu, C. Shen and H. Meng, *Adv. Sci.*, 2017, **4**, 1700335.
31 H. Shi, X. Zhang, X. Sun and X. Zhang, *Nanoscale*, 2018, **10**, 9892–9898.
32 Y. Chen, S. R. Smock, A. H. Flintgruber, F. A. Perras, R. L. Brutchey and A. J. Rossini, *J. Am. Chem. Soc.*, 2020, **142**, 6117–6127.
33 T. Hu, D. Li, Q. Shan, Y. Dong, H. Xiang, W. C. H. Choy and H. Zeng, *ACS Mater. Lett.*, 2021, **3**, 1702–1728.
34 H. Lu, A. Krishna, S. M. Zakeeruddin, M. Gratzel and A. Hagfeldt, *iScience*, 2020, **23**, 101359.
35 C. Li, S. Tscheuschner, F. Paulus, P. E. Hopkinson, J. Kiessling, A. Kohler, Y. Vaynzof and S. Huettner, *Adv. Mater.*, 2016, **28**, 2446–2454.
36 Q. A. Akkerman, G. Raino, M. V. Kovalenko and L. Manna, *Nat. Mater.*, 2018, **17**, 394–405.
37 J. Ye, M. M. Byranvand, C. O. Martinez, R. L. Z. Hoye, M. Saliba and L. Polavarapu, *Angew. Chem., Int. Ed.*, 2021, **60**, 21636–21660.
38 L. Yang, T. Wang, Q. Min, B. Liu, Z. Liu, X. Fan, J. Qiu, X. Xu, J. Yu and X. Yu, *ACS Omega*, 2019, **4**, 6084–6091.
39 L. Yang, H. Zhang, M. Zhou, L. Zhao, W. Chen, T. Wang, X. Yu, D. Zhou, J. Qiu and X. Xu, *J. Phys. Chem. Lett.*, 2020, **11**, 9203–9209.
40 M. I. Dar, G. Jacopin, S. Meloni, A. Mattoni, N. Arora, A. Boziki, S. M. Zakeeruddin, U. Rothlisberger and M. Grätzel, *Sci. Adv.*, 2016, **2**, e1601156.
41 B. Wu, H. Yuan, Q. Xu, J. A. Steele, D. Giovanni, P. Puech, J. Fu, Y. F. Ng, N. F. Jamaludin, A. Solanki, S. Mhaisalkar, N. Mathews, M. B. J. Roeffaers, M. Gratzel, J. Hofkens and T. C. Sum, *Nat. Commun.*, 2019, **10**, 484.
42 J. Kim, C. H. Chung and K. H. Hong, *Phys. Chem. Chem. Phys.*, 2016, **18**, 27143–27147.

 This journal is © The Royal Society of Chemistry 2023